Fuzzy Committees of Conceptual Distributed Model

Farrag, Mostafa; Perez, Gerald A.Corzo; Solomatine, Dimitri P.

DOI
10.1002/9781119639268.ch4

Publication date
2023

Document Version
Final published version

Published in
Advanced Hydroinformatics

4

FUZZY COMMITTEES OF CONCEPTUAL DISTRIBUTED MODEL

Mostafa Farrag[1,2,3], Gerald A. Corzo Perez[4], and Dimitri P. Solomatine[4,5,6]

[1] Department of Water Quality and Ecology Software, Deltares, Delft, The Netherlands
[2] Hydrology Section, GFZ German Research Centre for Geoscience , Potsdam, Germany
[3] In titute for Environmental Sciences and Geography, University of Potsdam, Potsdam, Germany
[4] IHE Delft Institute for Water Education, Delft, The Netherlands
[5] Water Resources Section, Delft University of Technology, Delft, The Netherlands
[6] Water Problems Institute of the Russian A ademy of Scien es, Moscow, Russia

Conceptual hydrological models imply a simplification of the complexity of the hydrological system; however, they lack the flexibility in reproducing a wide range of the catchment responses. Usually, a trade-off is done to sacrifice the accuracy of a specific aspect of the system behavior in favor of the accuracy of other aspects. This study evaluates the benefit of using a modular approach, "The fuzzy committee model" of building specialized models to reproduce specific responses of the catchment. We also assess the applicability of using predicted runoff from specialized models to form a fuzzy committee model. In this paper, weighting schemes with power parameter values are

Advanced Hydroinformatics: Machine Learning and Optimization for Water Re ource , Special Publication 78
Fir t Edition. Edited by Gerald A. Corzo Perez and Dimitri P. olomantine.

DOI: 10.1002/9781119639268.ch4

investigated. A thorough study is conducted on the relation between the fuzzy committee variables (the membership functions and the weighting schemes), and their effect on the model performance. Furthermore, the Fuzzy committee concept is applied on a conceptual distributed model with two cases, the first with lumped catchment parameters and the latter with distributed parameters. A comparison between different combinations of the fuzzy committee variables showed the superiority of all Fuzzy Committee models over single models. Fuzzy committee of distributed models performed well, especially in capturing the highest peak in the calibration data set; however, it needs further study of the effect of model parameterization on the model performance and uncertainty.

4.1. Introduction

Conceptual models are a handy tool as they provide a simplified description of the complexity and heterogeneity of reality· consequently, they produce only a narrow range of catchment response, and the accuracy in reproducing a specific behavior may come against the accuracy of other a pects (Fenicia et al., 2007). Using hydrological models with the best set of parameter results from the calibration of a single objective function might not capture the complexity of the rainfall-runoff relationship in all ranges of flow.

The source of error in conceptual models as described by Agawa and Takeuchi (2016) is that the model structure is not correct to some extent even with optimization. Furthermore, parameter values obtained using a real measurement or estimated from equations differ from values that would achieve an optimal fit. Besides, the spatial variation in both climate variables and catchment characteristics are ignored (Beven, 1996).

The rainfall-runoff relationship is very complex and characterized by highly variable spatial and temporal properties. According to Fenicia et al. (2007), catchment behavior may display different states characterized by phenomena that can generally be identified qualitatively but are challenging to be quantified. Some of these phenomena are seasonality effects due to vegetation, land cover, changes in the topsoil, which affect processes like interception and infiltration. Therefore, catchment response are season dependent.

Furthermore catchment hydrological states are the main driving forces for the catchment responses. Changes in the hydrological state could change the catchment conditions from dry to wet or high to low flow. The changes also affect the contributing area (saturated areas close to the river streams) to discharge leading to a change in the domain of the hydrological proces e . Last, most hydrological processes are characterized by nonlinear behavior like rainfall intensities groundwater level and soil moisture conditions. These processes in return control the surface runoff. fa t and low runoff response.

Calibration of rainfall-runoff models depends mainly on the objective function used during calibration and, therefore different objective function results in different parameter ets. Having more than one set of parameters for one catchment violates the model s physical ju tification which ideally should have one unique parameter et (Oudin et al. 2006). The unavoidable dependency of calibration on objective function can be turned into a solution to the different state of the catchment re ponses. Hence objective function can be adjusted to handle the practical issue for which the model is built.

By acknowledging the limitations of the conceptual models Corzo and Solomatine (2007), Fenicia et al. (2007) Fernando et al. (2009) and Oudin et al. (2006) have proposed approaches for the representation of a catchment behavior. Instead of searching for the best model to represent the whole domain in rainfall-runoff relation runoff can be categorized into different flow regimes, and different models can be calibrated to reproduce each regime (Fig. 4.1). Such specialized models then can be dynamically combined to establish a more comprehensive representation of the catchment processes. This approach is called the *modular* or *multimodel* approach and is considered one way of adding hydrological knowledge into models (Corzo & Solomatine 2007). The multimodel approach can implicitly consider the variability in the behavior of the catchment response that is not explicitly taken into account in the conceptual model realization.

The modular approach consider switching between different model representing different aspects of sy tem behavior. Therefore these models have to address different range of the flow hydrograph (Abrahart & See 2000) or different seasons. Based on Corzo and Solomatine (2007), the flow hydrograph was partitioned using three different method : clu tering-based classification baseflow separation and temporal segmentation. Jain and Sriniva ulu (2006) have decompo ed the hydrograph into different segments relying on the concept that different physical

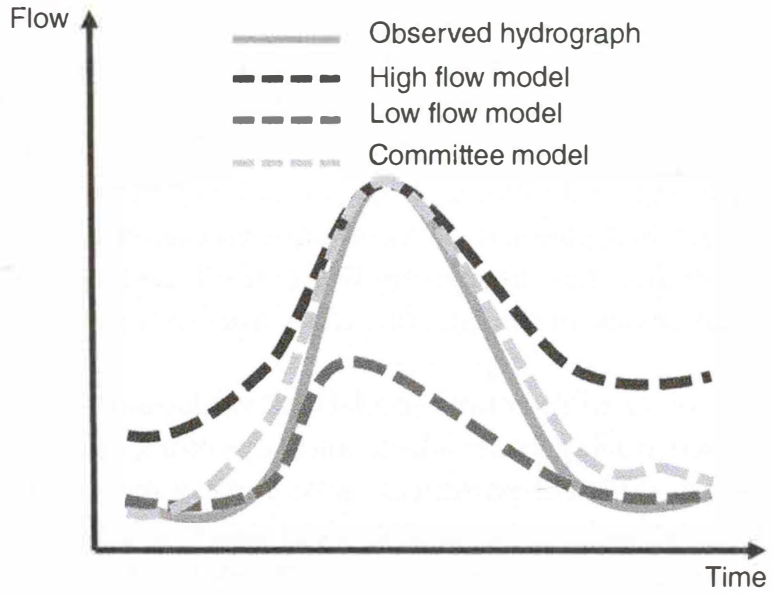

Figure 4.1 The concept of building local models represents different flow regimes and combining the flow simulated by these models using fuzzy membership function.

processes generate different hydrograph segments. Using multi-objective optimization to address different targeted hydrological responses (high and low flow) will result in a set of optimal solutions called *Pareto front*. The Pareto front represents a trade-off between the selected objectives. None of the optimization objectives can be further improved without the degradation of the other.

To incorporate the hydrological knowledge encapsulated in each of these specialized local models, Clemen (1989) has explored different architectures to combine models and forecasts; Jain and Srinivasulu (2006) have used a straightforward switching between models at different time steps. Various ways have been proposed to include a system of weighing, which can be very simple like the averaging method by Shamseldin et al. (1997) or a more complex technique (Ajami et al., 2006; Duan et al., 2007; Shamseldin et al., 1997; Xiong et al., 2001). The Bayesian model averaging scheme (BMA) (Duan et al., 2007) exploits predictions made by different hydrological models to form a probabilistic prediction. BMA weighs different models based on their probabilistic likelihood measures. Xiong et al. (2001) applies the Takagi-Sugeno fuzzy system (Takagi & Sugeno, 1985) to combine forecasted discharge from different models. Specialized models can also be combined based on a membership function. Membership function gives each model a different weight at every time step based on the runoff status (Kayastha et al., 2013). Models can also

be combined using a time-varying seasonal index extracted from a state variable or climatic data to weigh the specialized models (Oudin et al., 2006).

The fuzzy committee approach by Solomatine (2006) uses a membership function to express the difference in the degree of believability of the outputs of two models (high and low flow models). The membership function allows for a soft combination of models' output and prevents unrealistic discontinuities in the simulated system behavior (Fig. 4.1).

This research explores the fuzzy committee models first presented by Solomatine (2006) and further developed by Fenicia et al. (2007) and Kayastha et al. (2013), by building and combining different specialized models across weighting schemes and membership functions. In this chapter, different fuzzy committee model setups are tested with different goodness of fit. As recommended by Kayastha et al. (2013), weighting schemes with a power parameter of a value of 2 and 3 are considered. A thorough study is performed on the relation between the fuzzy committee parameters (the membership function (gamma, delta), the weighting schemes' type, and power parameter) and their effect on the model performance. The fuzzy committee concept is applied to a conceptual distributed model. Two cases are considered. The first uses lumped catchment parameters where two specialized models represent the whole catchment. The second uses distributed parameters where each cell is represented by two specialized models.

4.2. Case Study

The study catchment is in the Jiboa River in the central part of El Salvador. The catchment spreads over 432 km^2 with the outlet stations Puente Viejo located at (13.52 °N 88.98 °W) (Fig. 4.2). The catchment consists of four topographical areas: (1) San Vicente Volcano with an elevation of 2,171 m a.s.l (above sea level) and very steep slopes, (2) the Ilopango Lake (covers an area of 70 km^2) (3) the Balsamo mountain range area with an elevation of 1,000 m a.s.l, and (4) the coastal plain area with elevation ranges from 0 to 100 m a.s.l.

The basin is instrumented by a telemetry system of 15 min time step rainfall gauges and a water level gauge at the outlet of the catchment. For calibration of the model, rainfall and water level value were aggregated to the hourly time step while the water level was further converted into discharge using a rating curve equation. Monthly potential evapotranspiration values were obtained for each station using a potential evapotranspiration-elevation relation derived by Hargreaves method and

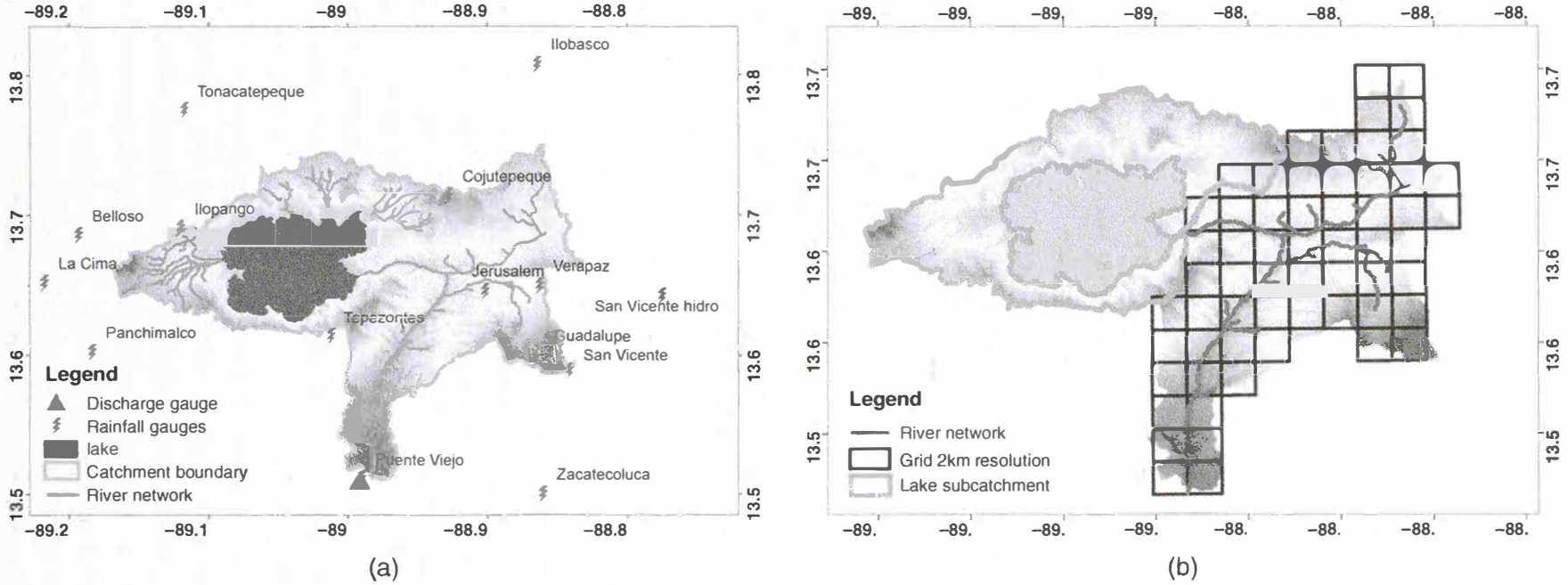

Figure 4.2 (a) Jiboa catchment stations and (b) model setup.

linear regression (SNET, 2005). Hourly temperature estimates were calculated from one available daily station using the sine function and were used for the whole catchment. The lake is simulated using a storage-outflow relation, where storage changes from inflow direct rainfall and evaporation are updated each time step. Outflow from the lake is calculated using the newly calculated storage. Inverse square distance weighting method was used to calculate distributed data for different spatial resolution for all data required for the hydrological imulation (precipitation, temperature potential evapotranspiration).

4.3. Methodology

The first step in building a fuzzy committee is hard partitioning, where a pareto-optimal set of specialized nondominated models is created via multi-objective optimization. Out of many possible models generated, those better representing high and low regimes are selected. The first step results in two pecialized high and low flow models addressing the catchment respon e they are built to reproduce. The second step is combining the imulated discharge from each model developed in the first step, using a fuzzy membership function. The fuzzy membership function consi ts of two parameters γ and σ whose values are obtained using optimization· the result of this step will be one imulated di charge output. (see Fig. 4.3). The term *committee model* will refer to a committee of two specialized models for low and high flow combined u ing a weighting scheme with optimized values of γ and δ to minimize the value of RMSE.

4.3.1. Model Structure Description

HBV-96 lumped conceptual model (Lind tröm et al. 1997) is u ed in this study to simulate the vertical movement of water for each cell/subcatchment. The ra ter-based distributed model is built where runoff from each cell is routed directly to the outlet using the Maxba function (Fig. 4.4)· each cell has a MAXBAS value depending on its flow path length. Discharge at the outlet is obtained by summing the routed runoff from all cells at each time step. Only uperficial discharge (surface runoff and interflow generated from upper zone UZ re ervoir in the HBV model structure) is routed, while flow generated from lower zone LZ i assumed to be lumped for the whole catchment (Fig. 4.4).

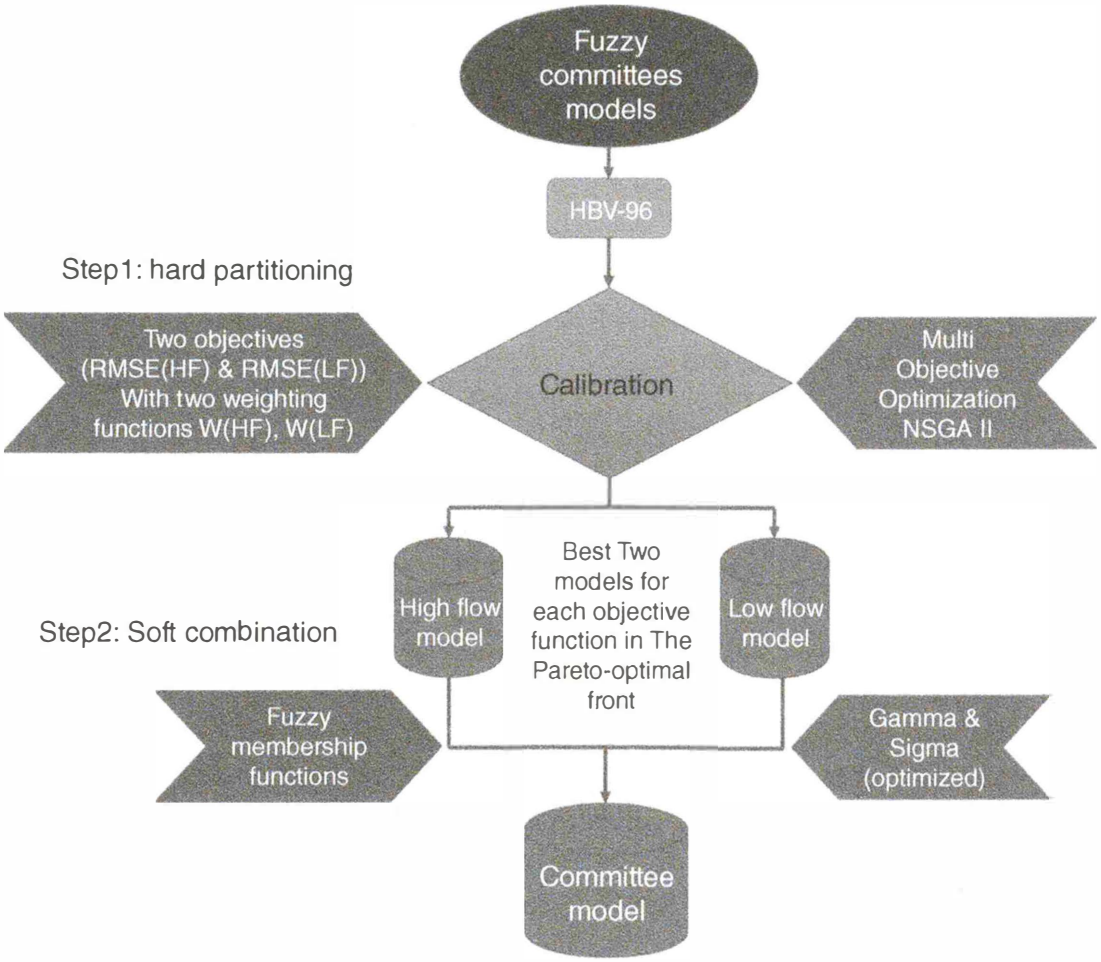

Figure 4.3 Proposed steps and approaches for improving committee models using a dynamic weighting scheme.

Several trials have been made to adapt the model structure to the spatial separation of the hydrological process, which happens when using the distributed model, as stated by Dehotin and Braud (2008). The beta parameter is responsible for passing water to the upper zone (equation (4.1)). To increase the sensitivity of the model structure to catchment fast response, beta is considered in the calibration with a value greater than 1. Additionally, a direct runoff rule is added to move water from the soil moisture tank to the upper zone whenever soil moisture exceeds the soil's field capacity (Schumann, 1993).

$$\frac{\mathrm{R}}{IN} = \left(\frac{SM}{FC}\right)^{\beta}. \tag{4.1}$$

R: Rainfall
EA: Actual evapotranspiration
FC: Field capacity
SM: Soil moisture
Inf: Infiltration
Cflux: capillary flux
Perc: Percolation
Q overland: Direct runoff
QUZ: Upper zone discharge
QLZ: Lower zone discharge
UZ: Upper zone storage
LZ: Lower zone storage
K, Kl: Upper and lower zone coefficients
α: Power coefficient

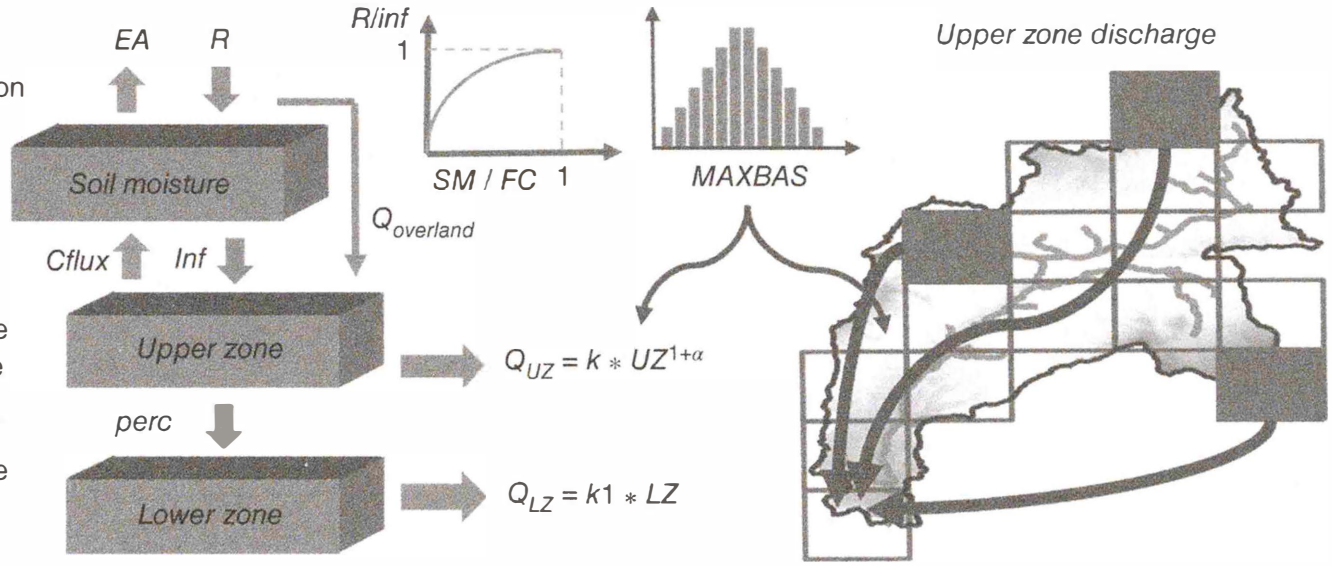

Figure 4.4 Model structure.

4.3.2. Model Calibration and Building Specialized Local Models

Model calibration follows a multi-objective optimization using the nondominated sorted genetic algorithm NSGA-II by Deb et al. (2002), where different objective functions are used as introduced by Gupta and Sorooshian (1998). The result of the multi-objective optimization is a pareto-optimal set of specialized models, which are nondominated solutions, and all are equally important. Having more than one solution indicates the conflicting nature of solutions, stating that optimal performance in one objective is paid in terms of suboptimal performance in other objectives. Every solution has its limitations and strengths in reproducing different catchment responses as a reflection of the associated objective function.

Model performance is always measured based on how close the simulated flow to the observed hydrograph is and how much the model succeeds in reproducing the streamflow volume correctly. Therefore, high and low flow were selected as distinct flow regimes and states of the system behavior; if the model managed to capture both states, the overall performance would be improved. The objectives of the modular model are to reproduce the system behavior during both regimes as accurately as possible. Root mean square error (RMSE) with W_{hf} and W_{lf} as weighting schemes (equations (4.2) and (4.3)) were used to put a higher emphasis on high and low flow values, respectively.

$$\mathrm{RMSE}_{hf} = \sqrt{\frac{1}{n}\left(\sum_{i=1}^{n}((\mathrm{Qobs}_i - \mathrm{Qsim}_i))^2 * W_{hf,i}\right)} \tag{4.2}$$

and

$$\mathrm{RMSE}_{lf} = \sqrt{\frac{1}{n}\left(\sum_{i=1}^{n}((\mathrm{Qobs}_i - \mathrm{Qsim}_i))^2 * W_{lf,i}\right)}, \tag{4.3}$$

where $Qobs_i$ and $Qsim_i$ are the observed flow and simulated flow respectively at each time step, W_{lf} and W_{hf} are the two weighting functions, with W_{lf} to place high weights on low flow and low weights on high flow values and W_{hf} to place stronger weights on high flow and weaker weights on low flow values on the hydrograph. The objective function, together with the weighting function, will be referred to as a weighting scheme (WStype), the corresponding figures and equation for each WStype are below (Fig. 4.5, Table 4.1)

Table 4.1 Weighting schemes for root mean square error for high ($RMSE_{hf}$) and low flow ($RMSE_{lf}$).

WStype	W_{lf}	W_{hf}	Eq	Figure
I	$=(l)^N$	$=(h)^N$	4.4	Figure 4.5a
II	$\begin{cases} 0, if\ l > \alpha \\ \left(\left(\frac{1}{\alpha^2}\right) * (1-l)^2 - \left(\frac{2}{\alpha}\right) * (1-l) + 1\right), if\ l \le \alpha \end{cases}$	$\begin{cases} 1, if\ h > \alpha \\ (h/\alpha)^N, if\ h \le \alpha \end{cases}$	4.5	Figure 4.5b
III	$\begin{cases} 0, if\ l > \alpha \\ \left(\left(\frac{1}{\alpha^2}\right) * (1-l)^2 - \left(\frac{2}{\alpha}\right) * (1-l) + 1\right), if\ l \le \alpha \end{cases}$	$\begin{cases} 1, if\ h > \alpha \\ 0, if \le \alpha \end{cases}$	4.6	Figure 4.5c
IV	$\begin{cases} 0, if\ l > \alpha \\ \left(1 - \left(\frac{1+1}{\alpha}\right)\right), if\ l \le \alpha \end{cases}$	$\begin{cases} 1, if\ h > \alpha \\ 0, if \le \alpha \end{cases}$	4.7	Figure 4.5d

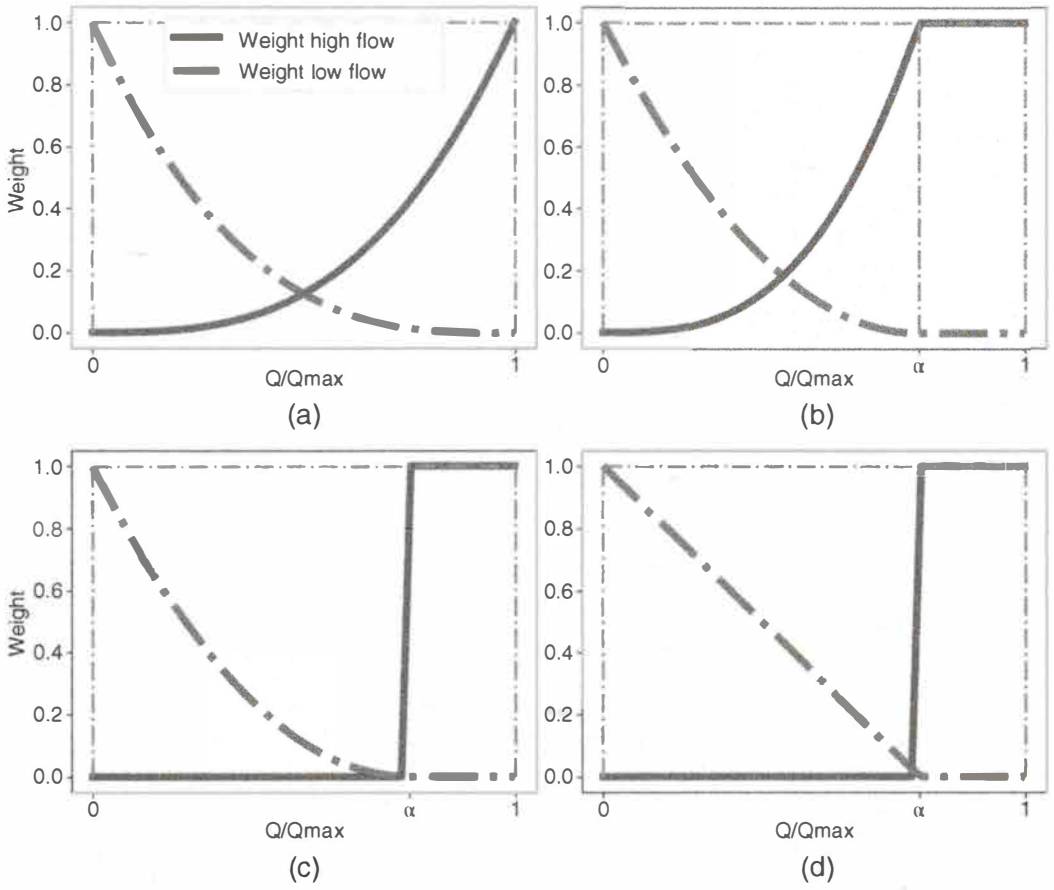

Figure 4.5 Weighting schemes for weighted root mean squared error as an objective function. W_{lf} and W_{hf} are obtained from equations (4.4)–(4.7): (a) WS-I, (b) WS-II, (c) WS-III, and (d) WS-IV.

l and h in the previous equations are calculated as equation (4.8):

$$l = \frac{(Q_{obs,max} - Q_{sim,i})}{Q_{obs,max}}, \quad h = \frac{Q_{obs,i}}{Q_{obs,max}}, \tag{4.8}$$

where $Q_{obs,\,max}$ is max observed flow value, α is a threshold for selecting weights, N is the power (see Table 4.1). N was chosen to be 2 ans 3, the value of α is a ratio between calculated discharge at a particular time step and the maximum discharge value in the calibration data set ($Q_i/Q_{obs,\,max}$). α, determines the range of values where both models are working together, and the range where discharge value from the high flow model is only considered, α was chosen to be 0.75.

It is important to mention that the values of $RMSE_{lf}$, $RMSE_{hf}$, and *RMSE* are calculated differently and cannot be compared with each other, as they have been multiplied by different weights. $RMSE_{lf}$ evaluates the error in low flow and $RMSE_{hf}$ evaluates the error in high flow, while RMSE

evaluates the error in the general flow. Data used in the calibration are almost 2 yr and a half-hourly time step, two wet seasons were used in the calibration data set and one in the validation.

4.3.3. Combining Specialized Models

The main objective is to produce a flow simulation efficient in both low and high flow domains using time-varying weights, as mentioned earlier. Obtaining a competent solution in all flow regimes is very difficult, and using a specialized model in both high and low flow is a better way to achieve a general efficient model.

The challenge in combining different specialized models built under different flow regimes is to determine which model will work and how to switch smoothly from one model to another carrying the water balance information; and in case more than one model is working at a time, how to handle the compatibility at the boundaries.

In order to avoid such complication, using a weighting scheme, which guarantees a smooth transition between models, can be the solution. The share of each specialized model will be determined using a fuzzy membership function described by Fenicia et al. (2007), Kayastha et al. (2013), and Solomatine (2006).

In the weighting scheme, a trapezoidal function with two parameters γ and δ is used, wherein the membership function of the low flow model a weight of 1 will be given to low flow values if the relative flow is below parameter γ (Fig. 4.6c), then starts to decrease when relative flow values are between γ and δ (both models are working together), until it reaches zero beyond the boundary of parameter δ (Fig. 4.6c). Similarly, the membership function of a high flow model is working but in opposite logic. The membership functions are shown here (equations (4.9) and (4.10)).

$$M_{lf} = \begin{cases} 1, if\, h < \gamma \\ 1 - \left(\dfrac{(h-\gamma)}{(\delta-\gamma)} \right)^{N}, if\, \gamma \le h \le \delta \\ 0, if\, h \ge \delta \end{cases} \tag{4.9}$$

and

$$M_{hf} = \begin{cases} 0, if\, h < \gamma \\ \left(\dfrac{(h-\gamma)}{(\delta-\gamma)} \right)^{1/N}, if\, \gamma \le h \le \delta \\ 1, if\, h \ge \delta \end{cases} \tag{4.10}$$

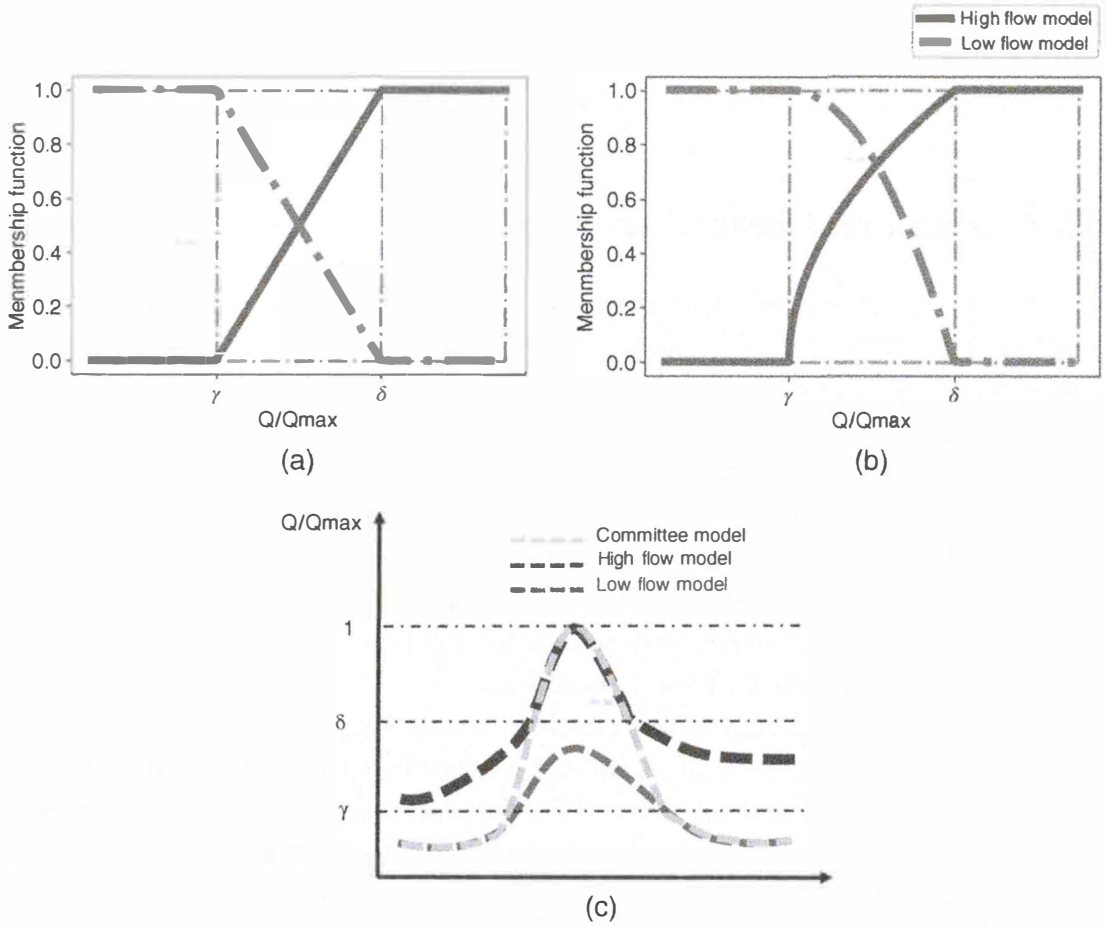

Figure 4.6 Fuzzy membership functions to combine specialized models: (a) MF-A uses a linear transition between γ and σ threshold (N equals 1); (b) MF-B uses nonlinear transition with N equals 2; (c) segments of the hydrograph where each part of the membership function is applied.

The output of the two specialized models is multiplied by the previous weights and then normalized, so the final calculated flow from the committee models will be as follows (equation (4.11)). The combining function of high and low flow specialized models

$$Q_{C,i} = \frac{M_{lf,i} * Q_{lf,i} + M_{hf,i} * Q_{hf,i}}{M_{lf,i} + M_{hf,i}}, \tag{4.11}$$

where $Q_{LF,i}$ and $Q_{hF,i}$ are simulated high and low flows, respectively; M_{LF} and M_{hF} are membership functions for low and high flow models, respectively; i is the time step; and γ and δ are two thresholds for low and high flows, respectively. N is the power value to smooth the transition between models; for Type A, N is equal to one, for Type B, N is equal to two (see Fig. 4.6).

The γ and σ are the membership function thresholds that represent switches in the catchment behavior; these switches ould be a reflection of change in contributing area that feeds the outflow or change in the channel properties (Fenicia et al. 2007).When there is no way to quantify the change in the catchment behavior into thresholds γ and σ could be determined using optimization to minimize the root mean squared error of the committee model.

4.3.4. Model Setup

Different spatial setups were used to simulate the hydrological response of the catchment. The presence of the lake prevented the representation of the whole catchment using one lumped model. Therefore, the lake and all the upstream subcatchments to the lake were represented as one lumped model (Fig. 4.2), which will be referred to as lake subcatchment. Different spatial resol tions are used to simulate the rest of the catchment (which will be referred to as the Jiboa subcatchment) in order to capture the spatial variability of the precipitation. Jiboa subcatchment is simulated using different model setups as follows:

1. Lumped model (two models in total)
2. Committee of specialized lumped model (Lumped-MF-A and Lumped-MF-B) where two model are combined using two different membership functions (four models in total, two specialized models for each subcatchment).
3. Conceptual distributed model built with lumped catchment parameters (Dist-L) using different spatial resolutions (4 km, 2 km 1 km, and 500 m) (two models in total, one model for each subcatchment)
4. Committee of conceptual distributed models (Dist-L-C two specialized models for the entire subcatchment) built with lumped catchment parameters using a spatial resolution of $4\,km^2$ (four models in total, two specialized models for each subcatchment)
5. Conceptual distributed model built with distributed catchment parameters (Dist-D different parameter for each cell) using $4\,km^2$ spatial resolutions (one model for each cell and one model for the lake subcatchment)
6. Committee of conceptual distributed models (Di t-D-C two pecialized models for each cell) built with distributed catchment parameter using a spatiai resolution of $4\,km^2$ (two models for each cell and two specialized models for the lake subcatchment)

The lake subcatchment is represented the same way in all models, and the only difference between models is the spatial representation of the Jiboa subcatchment.

4.3.5. Evaluation Criteria

Different performance criteria were used to compare and assess the performance of each model: Nash-Sutcliffe efficiency coefficient (NSE) (equation (4.12)), Nash-Sutcliffe with logarithmic values (equation (4.13)), root mean square error (RMSE) (equation (4.15)).

$$\mathrm{NSE(HF)} = 1 - \frac{\sum_t (\mathrm{Qobs} - \mathrm{Qsim})^2}{\sum_t (\mathrm{Qobs} - \mathrm{Qavg})^2}. \tag{4.12}$$

As the standard formula of Nash-Sutcliffe overestimates high values, so changing the values of flow by logarithmic values (equation (4.13)) will flatten the high flow; the peaks and low flow values will be the same. As a result, the effect of the error in low flow values will dominate, and the error value will be more sensitive to error in low flow values (Krause et al., 2005).

$$NSE(lf) = 1 - \frac{\sum_t (\ln(Qobs) - \ln(Qsim))^2}{\sum_t (\ln(Qobs) - \ln(Qavg))^2}. \tag{4.13}$$

The mean cumulative error measures how much the model succeeds in reproducing the streamflow volume correctly (equation (4.14)).

$$WB = 100 * \left(1 - \left|1 - \frac{\sum Qsim}{\sum Qobs}\right|\right). \tag{4.14}$$

$$RMSE = \sqrt{\frac{1}{n}\sum_{i=1}^{n} (Qobs - Qsim)^2}. \tag{4.15}$$

Gupta et al. (2009) have shown the limitation of using a single error function to measure the efficiency of calculated flow and showed that Nash-Sutcliff efficiency (NSE) or RMSE could be decomposed into three components: correlation, variability, and bias. The KGE index (equation (4.16)) has aggregated this information into one formula, which measures how far the values of these properties to the ideal point.

$$KGE = 1 - \sqrt{(c-1)^2 + (\alpha - 1)^2 + (\beta - 1)^2}, \tag{4.16}$$

where *Qobs* is the observed discharge, *Qsim* is the simulated discharge, and *Qavg* is the mean of observed discharges, c = *cross correlation between*

Qobs & *Qsim*, α measures the variability in the data $\alpha = \frac{\sigma_{Qsim}}{\sigma_{Qobs}}$, and $\beta = \frac{\text{mean(Qsim)}}{\text{mean(Qobs)}}$.

4.4. Results and Discussion

The conceptual representation of the catchment responses in the HBV model does not allow for simultaneous optimal representation of various behaviors of the catchment response. Therefore, the committee model approach is used to capture simultaneously different aspects of the catchment behavior

For the lake subcatchment, two specialized models have been built and used for the whole study without change, while for the Jiboa subcatchment, different spatial discretization (lumped and distributed) were modeled using four different cell resolutions (4 km, 2 km, 1 km, and 500 m)(see Fig. 4.7 and section 4.3.4 Model Setup).

For the lumped representation of the Jiboa subcatchment, two specialized models have been built for each subcatchment (two models for lake subcatchment and two models for Jiboa subcatchment). The Table 4.2 shows a summary of the performance of a different combination of committee models.

The values of both gamma and delta in Table 4.1 are further visualized in Figure 4.8 to analyze the interaction between the weighting scheme, the membership function, and the power value N. Gamma and delta are values of discharge threshold that determine how much both specialized models are working together. Figure 4.8 shows that MF-A makes specialized models work together more as it goes from WS-1 to WS-IV (the length of the lines increase from WS-I to WS-IV). On the other side, MF-B and N = 2 for both WS-I and II specialized models are almost working individually (models works together only in the range of Q/Qmax between γ of 0.24 to δ of 0.27), while MF-B with WS-I, WS-II (N = 3), WS-III and IV make models work together most of the time (in the range of Q/Qmax between γ = 0.06 to δ = 0.88).

More comprehensive studying on the relation between membership function, weighting scheme, and power value (N) shows that MF-B tends to make specialized models either to work together all the time or to work almost individually, as shown in Figure 4.8, which gives higher values of errors as shown in Figure 4.9 (points with bigger size). MF-A makes specialized models work individually and together almost equal times (the difference between delta and gamma around 0.5), which gives better results for committee model performance.

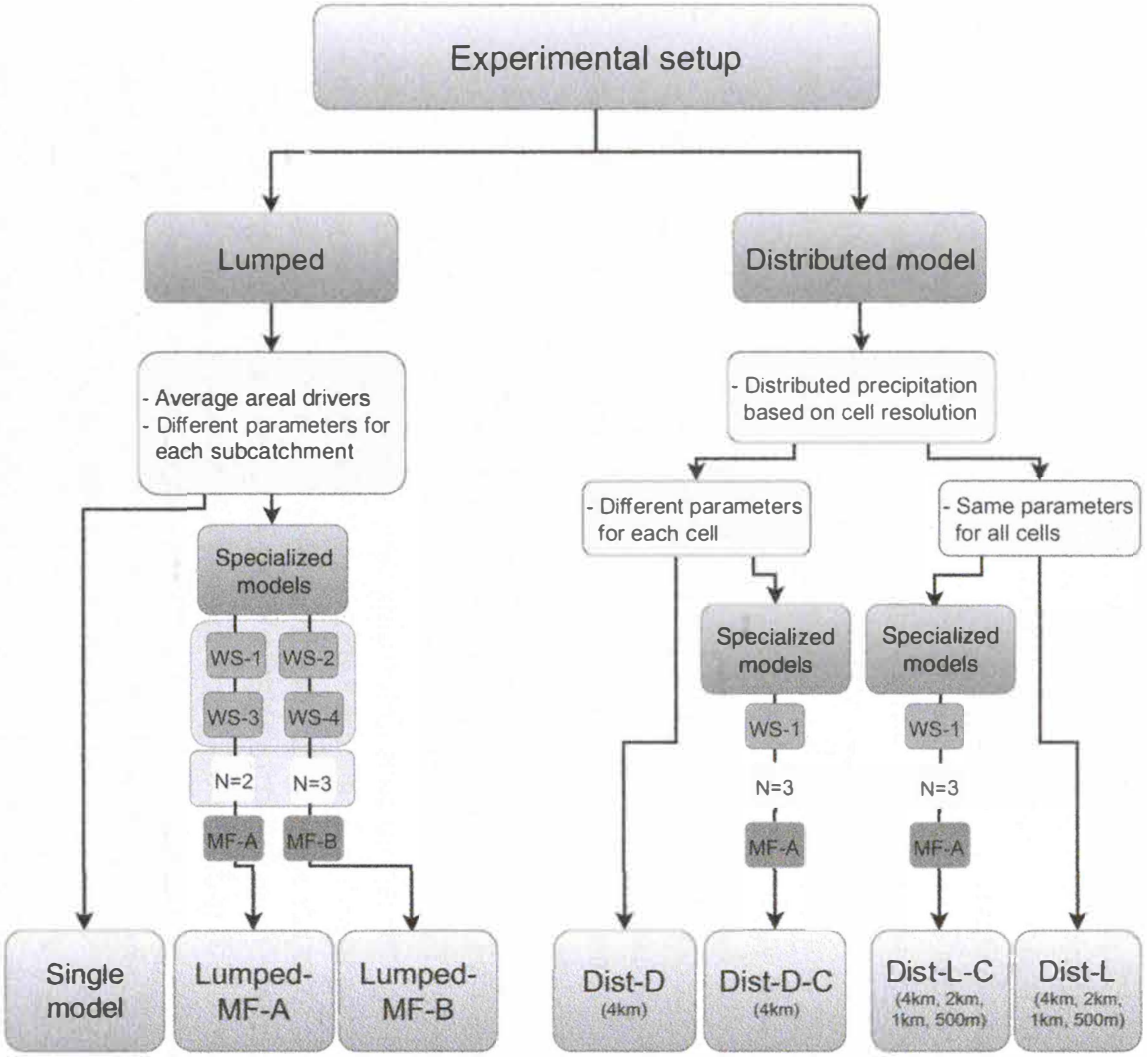

Figure 4.7 Experimental models setup.

Table 4.2 Performance of committee models with a different combination of weighting schemes and membership.

Model	WS type		Membership function			Low flow RMSE (lf)		High flow RMSE (Hf)		RMSE		KGE	
	WS type	N	MF	γ	Δ	Cal.	Val.	Cal.	Val.	Cal.	Val.	Cal.	Val.
	Single model					0.98	0.80	0.63	0.70	1.66	1.72	0.70	0.650
Committee model	I	2	A	0.19	0.36	0.95	0.84	0.58	0.71	1.36	1.45	0.84	0.84
			B	0.23	0.26	0.97	0.90	0.59	0.72	1.39	1.51	0.84	0.84
		3	A	0.17	0.43	0.80	0.68	0.42	0.47	1.28	1.34	0.88	0.87
			B	0.08	0.79	0.83	0.64	0.44	0.45	1.33	1.25	0.85	0.85
	II	2	A	0.15	0.35	0.80	0.65	0.75	0.88	1.33	1.37	0.85	0.83
			B	0.24	0.26	0.83	0.78	0.76	0.91	1.38	1.50	0.83	0.81
		3	A	0.18	0.41	0.81	0.70	0.60	0.73	1.28	1.41	0.87	0.86
			B	0.06	0.72	0.84	0.65	0.61	0.70	1.33	1.31	0.86	0.87
	III	-	A	0.16	0.57	0.82	0.67	0.35	0.29	1.31	1.28	0.87	0.87
			B	0.10	0.84	0.84	0.65	0.34	0.26	1.34	1.22	0.86	0.87
	IV	-	A	0.19	0.61	1.01	0.85	0.33	0.24	1.32	1.26	0.86	0.86
			B	0.13	0.87	1.03	0.79	0.34	0.24	1.35	1.18	0.86	0.90

Model	WS type		Membership function	Low flow NSE (ln)		High flow NSE		WB	
	WS type	N	MF	Cal.	Val.	Cal.	Val.	Cal.	Val.
Single model				0.6	0.821	0.615	0.691	99.48	85.08
Committee model	I	2	A	0.66	0.843	0.741	0.781	98.54	89.08
			B	0.66	0.82	0.731	0.762	99.02	89.09
		3	A	0.69	0.856	0.769	0.812	99.38	93.86
			B	0.68	0.864	0.750	0.836	99.89	87.57
	II	2	A	0.7	0.886	0.751	0.805	99.14	87.32
			B	0.69	0.84	0.734	0.764	97.35	85.08
		3	A	0.7	0.854	0.770	0.792	98.84	93.25
			B	0.69	0.862	0.752	0.820	97.05	91.25
	III	-	A	0.68	0.887	0.759	0.830	99.07	93.15
			B	0.68	0.885	0.749	0.844	99.42	88.93
	IV	-	A	0.66	0.893	0.755	0.833	96.23	96.48
			B	0.65	0.895	0.746	0.855	95.88	93.72

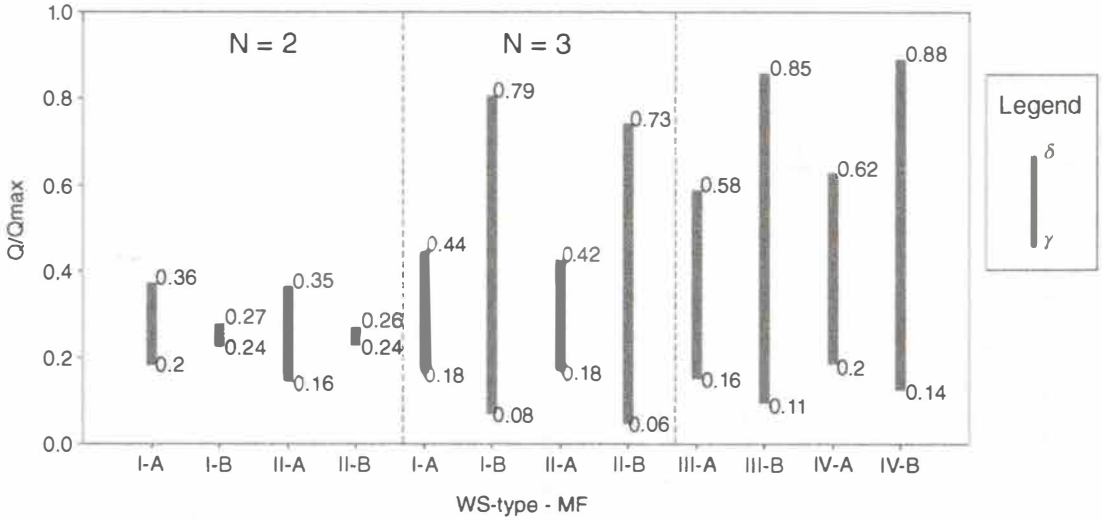

Figure 4.8 Weighting scheme parameters (gamma and delta). The first part of the x-axis notation represents the WS-type, and the second part represents the membership function. The figure is divided into parts based on the power N (WS-III and WS-IV do not have N). The line represents the range of discharge where both models (high and low flow models) are considered in the total calculated discharge for the committee model Qc (i.e., for WS I-A for Q/Qmax less than 0.2, only the low flow model is considered, and the opposite for Q/Qmax is greater than 0.36, while for Q/Qmax between 0.2 and 0.36, both models are considered in the Qc).

The weights W_{lf},W_{hf} are mainly affected by the proportional value of the calculated discharge to the maximum observed discharge during the calibration period ($Q_i/Q_{obs,max}$). Since $Q_{obs,max}$ depends on the chosen period of the calibration and can be surpassed in the validation data set or when the model is used in operation, then W_{lf} will have negative values. To avoid such a problem, a wider range of discharge could be used. Parameters obtained by the optimization algorithm are shown in Figure 4.10.

In Figure 4.10, the parameters' values are normalized with respect to the lower and upper bounds so that the feasible range of all parameters could be shown at the same figure between 0 and 1. Each line on the figure represents one set of parameters, and it indicates the relation between how the parameter range corresponds to the optimal solutions and the initial feasible parameter range. Any observations about the degree of variability of the parameters will not be in the right context as the figure represents only the values of the Pareto optimal set of solutions (see dark squares in Fig. 4.15), not all the solutions (other grey dots in Fig. 4.15).

The behavior of some parameters may follow a trend when moving from the best model for high flow to the best model for low flow; this behavior is evident in parameter K, which is the discharge coefficient of the upper

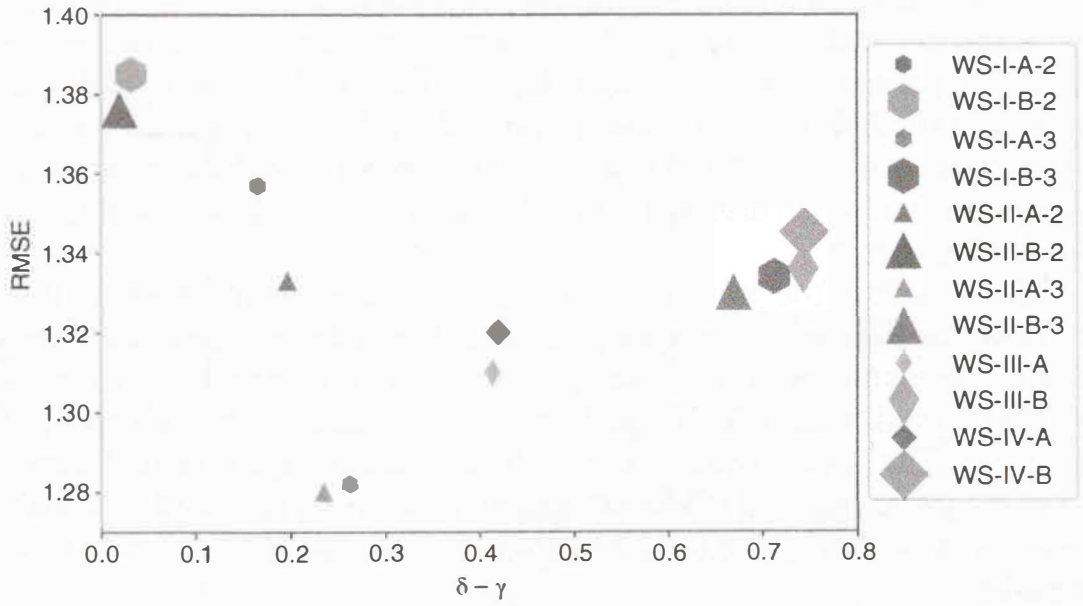

Figure 4.9 The relation between committee component and committee model performance, the first part of the points' notation, refers to the WS-type; the second part refers to the membership function (A or B); and the last part represents the power N (WS-III and WS-IV do not have N).

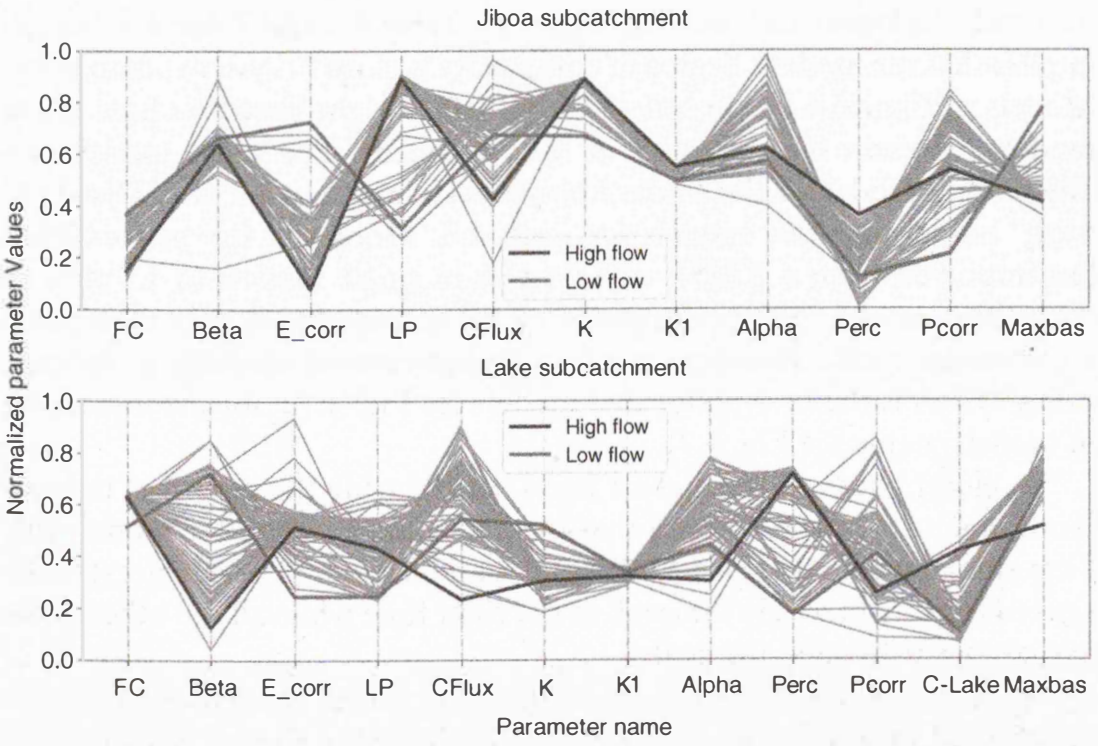

Figure 4.10 Normalized parameters plot (parameters corresponding to Pareto optimal solutions).

zone (subsurface flow) and K1 the discharge coefficient of the lower zone (groundwater flow). As expected the high flow model overestimate the values of parameter K K1, and C-lake as the trend of the model i to maximize the flow to get as close as possible to high flow values and the opposite for low flow. K1 and C-lake coefficients determine the lower reservoir's behavior, which dominates the respon e of the catchment during low flow simulation.

As a result of the previous behavior, it was expected to have high flow and low flow hydrograph encompassing the observed flow hydrograph (high flow is upper and low flow i lower), but this does not happen as explained by Oudin et al. (2006). This could happen in ideal case but not most of the case . The reason could return to the existence of a lake that dominates the lower response of the catchment and during the low flow season (November to April), the total flow from the catchment comes only from the lake.

For conceptual distributed models specialized model have been built using weighting scheme 1 (N = 3) for every ingle cell in the Jiboa subcatchment. Membership function A was used to combine specialized models obtained earlier using two parameters gamma and delta obtained by optimization using root mean square as an objective function. The committee of distributed models performance shows very close result in both calibration and validation data set (see Fig. 4.11, Table 4.2 and Table 4.3) which implies that the models' degree of complexity is close to ystem complexity. Models in Figure 4.11 are ordered from left to right ba ed on how many models represent the responses of the catchment. The ingle model use one general model for the whole Jiboa subcatchment, while the "Di t-D-C 4 km" model uses two models for each cell. Moreover, the performance has improved from a RMSE of 1.64 m^3/s in single models to 1.3 m^3/s in committee models· the performance of all committees is very close; and a committee model repre ent.ing Jiboa subcatchment spatially as lumped using MF-A is the best-performed model (see Fig. 4.12· for the indication of models' name see Fig. 4.7).

A closer check to the highest flood event during the period of the calibration data set it was found that the distributed committee model with 4 km spatial resolution Dist-D-C 4 km (with distributed parameters) manages to capture precisely the peak at the right time while all the other committees overestimated the peak.

Figure 4.14 and Table 4.3 show the performance of all models, with a normalized value of all metrics. For RMSE RMSE(LF) and RMSE(HF) the highest error is at the top of the graph with a value of 1.656 1.05 and 0.64, respectively, and the lowest values at the bottom of the graph with values of 1.282, 0.8, and 0.43, respectively. While for NSE(HF) and

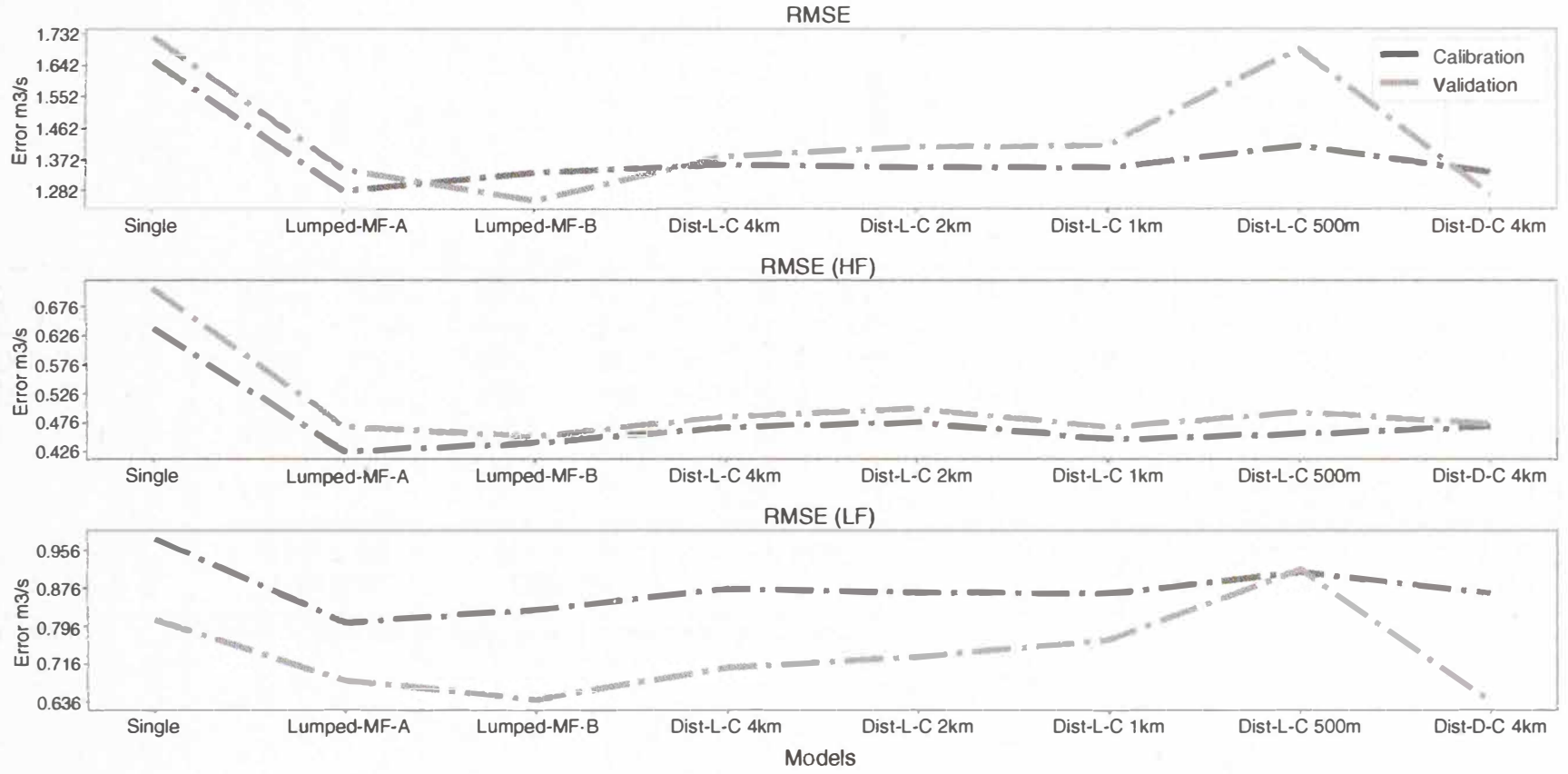

Figure 4.11 Performance graph of all committee models. Models are ordered from left to right based on how many models are used to represent the catchment.

Table 4.3 Committee of conceptual distributed models' performance.

Model name	Low flow RMSE (lf)		High flow RMSE (Hf)		RMSE		KGE		High flow NSE		Low flow NSE (ln)	
	Cal.	Val.	Cal.	Val.	Cal.	Val.	Cal.	Val.	Cal.	Val.	Cal.	Val.
Dist-L-C 4km	0.88	0.71	0.47	0.49	1.36	1.38	0.85	0.87	0.74	0.80	0.67	0.86
Dist-L-C 2km	0.87	0.73	0.48	0.50	1.35	1.41	0.84	0.86	0.74	0.79	0.68	0.85
Dist-L-C 1km	0.86	0.77	0.45	0.47	1.35	1.41	0.85	0.80	0.74	0.79	0.71	0.76
Dist-L-C 500m	0.91	0.92	0.46	0.49	1.41	1.69	0.79	0.79	0.72	0.70	0.66	0.78
Dist-D-C 4km	0.87	0.64	0.47	0.47	1.34	1.27	0.84	0.88	0.75	0.83	0.67	0.90

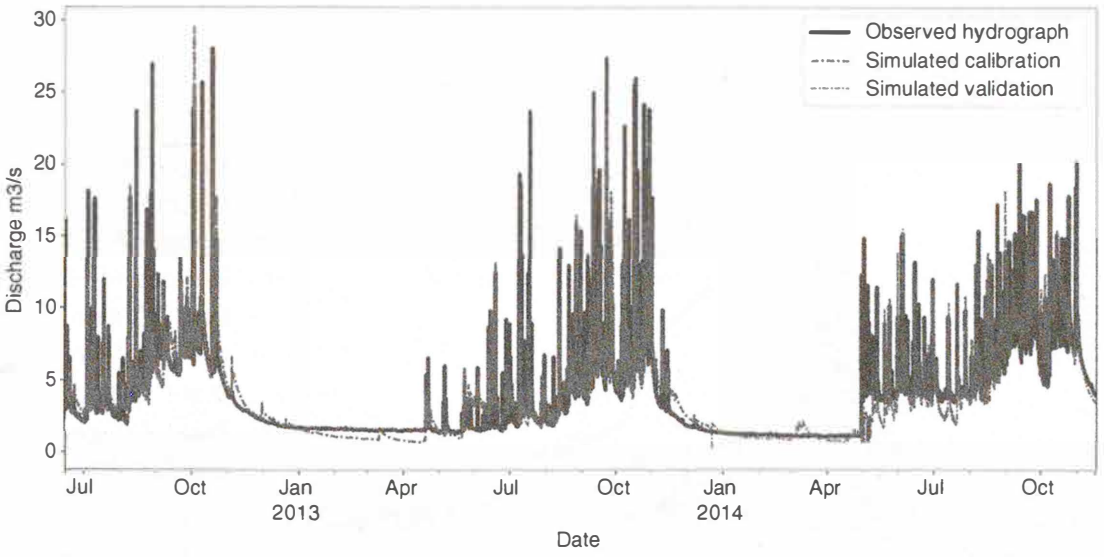

Figure 4.12 Flow hydrograph result from committee model Lumped-MF-A.

NSE(LF), the highest values are at the bottom of the graph with values of 0.71 and 0.77, respectively, and the lowest values at the top of the figure with values of 0.55 and 0.62, respectively. All single models (lumped and distributed) appear at the upper part of the figure (highest RMSE and lowest NSE) while committee models appear at the bottom of the graph (lowest RMSE and highest NSE), which indicates that committee models outperformed all single models in all performance criteria. Figure 4.13 with Figure 4.11 show that the effect of cells' size in distributed models is very slight, which indicates the need for more research regarding the conceptual distributed models.

The best 70 model parameterizations found by NSGA-II are presented in Figure 4.15 as a Pareto front of optimal nondominated solutions. It also illustrates the trade-off between selected objectives and indicates that the single models can not simultaneously match the full variability of the catchment response. The optimal set of parameters for the calibration data set does not have superiority over the validation data set, so the best-specialized models of high and low flow obtained for the calibration data set are not the best (among other Pareto optimal set) in the validation data set.

Figure 4.15 shows that committee models are closer to the ideal point than the single models and all members of the Pareto front. This ensures that committee models' performance is better than any other single model. The optimal models in calibration are not necessary to be the best in validation as well. However, the version in calibration and validation has to be very close. All combinations of committee models were better than all of Pareto members in both calibration and validation data sets.

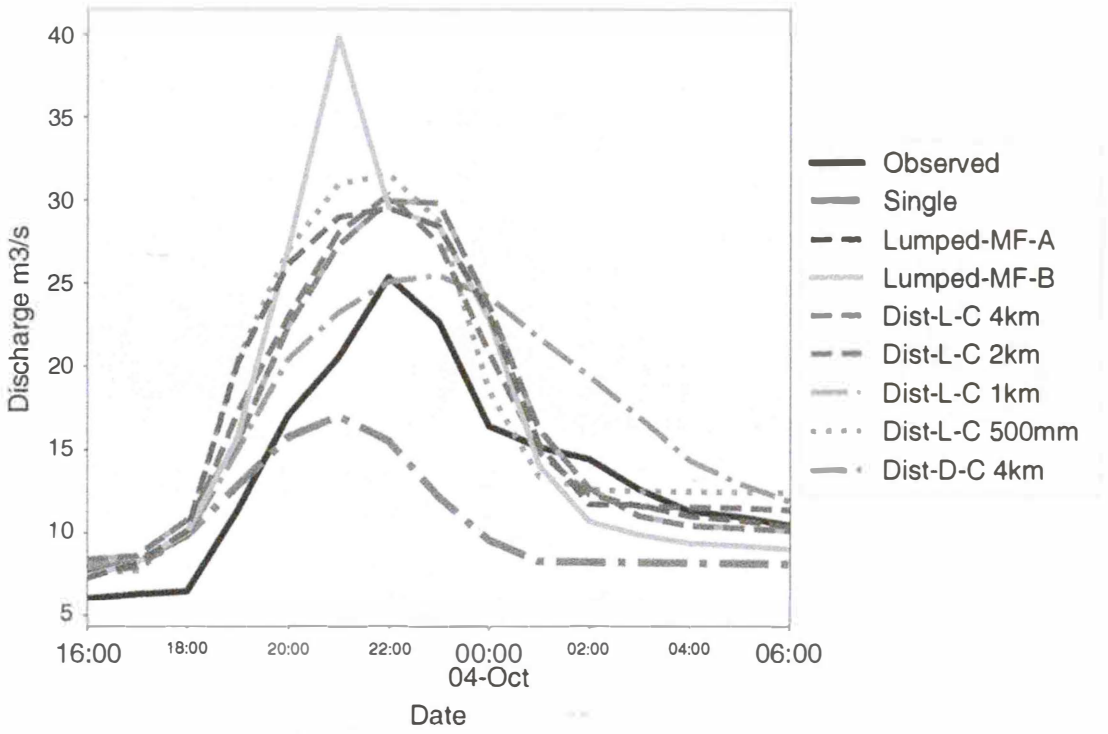

Figure 4.13 Performance of committee models at the highest flood event in the calibration period.

It is easily noticeable that the values of $RMSE_{LF}$ are always higher than the values of $RMSE_{HF}$. The reason is that the low flow period is much longer than the high flow period, so it is expected that longer periods would have higher error than shorter periods (the number of low flow values is more than high flow values) and the formula of weighted root mean squared error summation of the error is divided by the same total number of observations see (Fig. 4.15).

A committee of specialized models developed to reproduce a particular aspect of the hydrologic response (high and low flow models) combined using a fuzzy membership function managed to exploit the strength of each model to improve the performance of the committee. This gives the closest performance to the ideal point than all single models and all Pareto front members, which ensures that the committee models' performance is better than any other single model.

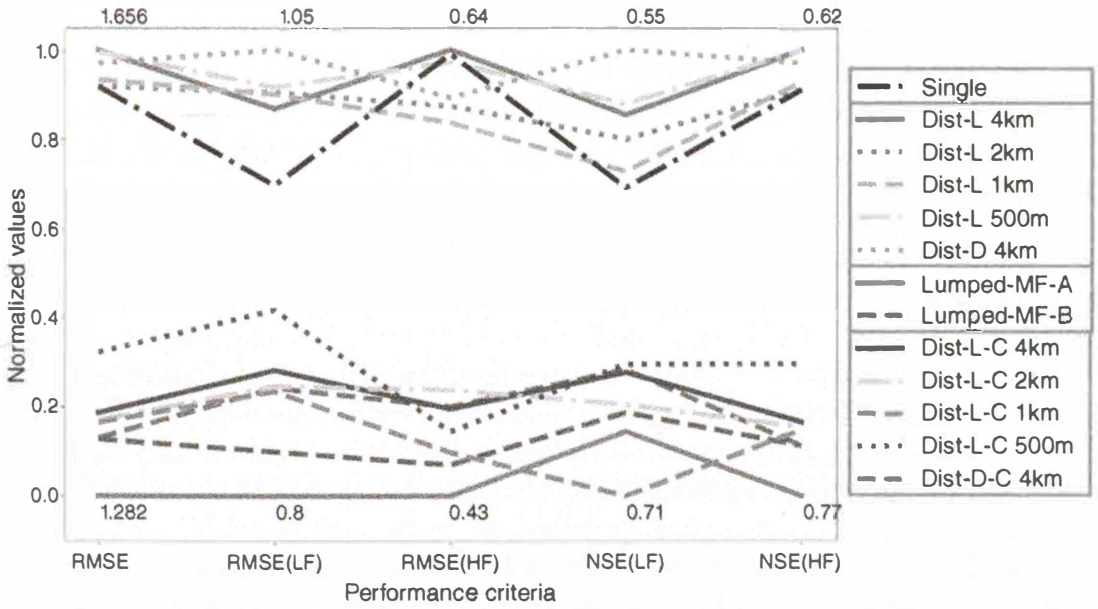

Figure 4.14 Normalized performance criteria of all models for the visual comparison, the maximum and minimum values of each error are presented. Committee models at the bottom have lower RMSE, RMSE(LF), and RMSE(HF), and higher NSE(LF) and NSE(HF); thus, the performance is better in all criteria.

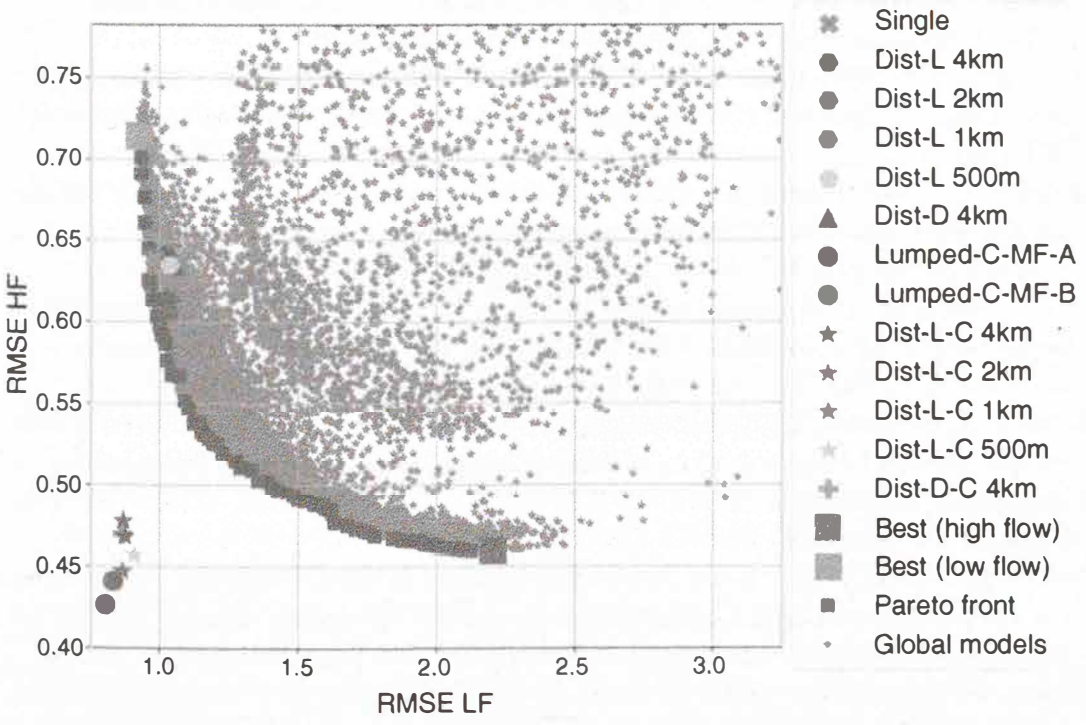

Figure 4.15 Pareto optimal sets of specialized models result from the multiobjective optimization and the different models.

Acknowledgments

We thank the Ministry of Environment and Natural resources of El Salvador (MSRN) for providing data used in this study. We also thank Rotary Foundation (TRF) for the fund provided within the Rotary fellowship.

References

Abrahart, R. J., & See, L. (2000). Comparing neural network and autoregressive moving average techniques for the provision of continuous river flow forecasts in two contrasting catchments. *Hydrological Processes*, *14*(11–12), 2157–2172. https://doi.org/10.1002/1099-1085(20000815/30)14:11/12<2157::AID-HYP57>3.0.CO;2-S

Agawa, T., & Takeuchi, O. (2016). Re-examination of psychological needs and L2 motivation of Japanese EFL learners: An interview study. *Asian EFL Journal*, *89*(89), 74–98.

Ajami, N. K., Duan, Q., Gao, X., & Sorooshian, S. (2006). Multimodel combination techniques for analysis of hydrological simulations: application to distributed model intercomparison project results. *Journal of Hydrometeorology*, *7*(4), 755–768. https://doi.org/10.1175/jhm519.1

Beven, K. (1996). *Equifinality and uncertainty in geomorphological modeling.* The Scientific Nature of Geomorphology. Proceeding of the 27th Binghamton Symposium in Geomorphology, *September 1996*, 289–314.

Clemen, R. T. (1989). Combining forecasts: A review and annotated bibliography. *International Journal of Forecasting*, *5*(4), 559–583. https://doi.org/10.1016/0169-2070(89)90012-5

Corzo, G., & Solomatine, D. (2007). Baseflow separation techniques for modular artificial neural network modeling in flow forecasting. *Hydrological Sciences Journal*, *52*(3), 491–507. https://doi.org/10.1623/hysj.52.3.491

Deb, K., Pratap, A., Agarwal, S., & Meyarivan, T. (2002). A fast and elitist multiobjective genetic algorithm: NSGA-II. *IEEE Transactions on Evolutionary Computation*, *6*(2), 182–197. https://doi.org/10.1109/4235.996017

Dehotin, J., & Braud, I. (2008). Which spatial discretization for distributed hydrological models? Proposition of a methodology and illustration for medium to large-scale catchments. *Hydrology and Earth System Sciences*, *12*(3), 769–796. https://doi.org/10.5194/hess-12-769-2008

Duan, Q., Ajami, N. K., Gao, X., & Sorooshian, S. (2007). Multimodel ensemble hydrologic prediction using Bayesian model averaging. *Advances in Water Resources*, *30*(5), 1371–1386. https://doi.org/10.1016/j.advwatres.2006.11.014

Fenicia, F., Solomatine, D. P., Savenije, H. H. G., & Matgen, P. (2007). Soft combination of local models in a multi-objective framework. *Hydrology and Earth System Sciences*, *11*(6), 1797–1809. https://doi.org/10.5194/hess-11-1797-2007

Fernando, D. A. K., Shamseldin, A. Y., & Abrahart, R. J. (2009). *Using gene expression programming to develop a combined runoff estimate model from conventional rainfall-runoff model outputs.* 18th World IMACS Congress and

MODSIM09 International Congress on Modeling and Simulation: Interfacing Modeling and Simulation with Mathematical and Computational Sciences, Proceedings, July, 748–754. https://www.scopus.com/inward/record.uri?eid=2-s2.0-80052983135&partnerID=40&md5=73dcd5eba92b4c026dcff2b6bf128f02

Gupta, H. V., & Sorooshian, S. (1998). Toward improved calibration of hydrologic models: Multiple and noncommensurable measures of information. *Water Resources Research*, *34*(4), 751–763.

Gupta, H. V., Kling, H., Yilmaz, K. K., & Martinez, G. F. (2009). Decomposition of the mean squared error and NSE performance criteria: Implications for improving hydrological modeling. *Journal of Hydrology*, *377*(1–2), 80–91. https://doi.org/10.1016/j.jhydrol.2009.08.003

Jain, A., & Srinivasulu, S. (2006). Integrated approach to model decomposed flow hydrograph using artificial neural network and conceptual techniques. *Journal of Hydrology*, *317*(3–4), 291–306. https://doi.org/10.1016/j.jhydrol.2005.05.022

Kayastha, N., Ye, J., Fenicia, F., Kuzmin, V., & Solomatine, D. P. (2013). Fuzzy committees of specialized rainfall-runoff models: Further enhancements and tests. *Hydrology and Earth System Sciences*, *17*(11), 4441–4451. https://doi.org/10.5194/hess-17-4441-2013

Krause, P., Boyle, D. P., & Bäse, F. (2005). Comparison of different efficiency criteria for hydrological model assessment. *Advances in Geosciences*, *5*(89), 89–97. https://doi.org/10.5194/adgeo-5-89-2005

Lindström, G., Johansson, B., Persson, M., Gardelin, M., & Bergström, S. (1997). Development and test of the distributed HBV-96 hydrological model. *Journal of Hydrology*, *201*(1–4), 272–288. https://doi.org/10.1016/S0022-1694(97)00041-3

Oudin, L., Andréassian, V., Mathevet, T., Perrin, C., & Michel, C. (2006). Dynamic averaging of rainfall-runoff model simulations from complementary model parameterizations. *Water Resources Research*, *42*(7), 1–10. https://doi.org/10.1029/2005WR004636

Schumann, A. H. (1993). Development of conceptual semi-distributed hydrological models and estimation of their parameters with the aid of GIS. *Hydrological Sciences Journal*, *38*(6), 519–528. https://doi.org/10.1080/02626669309492702

Shamseldin, A. Y., O'Connor, K. M., & Liang, G. C. (1997). Methods for combining the outputs of different rainfall-runoff models. *Journal of Hydrology*, *197*(1–4), 203–229. https://doi.org/10.1016/S0022-1694(96)03259-3

SNET (2005). *Balance hídrico integrado y dinámico en El Salvador*, 109. https://unesdoc.unesco.org/ark:/48223/pf0000228142

Solomatine, D. P. (2006). *Optimal modularization of learning models in forecasting environmental variables*. Proceedings of the IEMSs 3rd Biennial Meeting, Summit on Environmental Modeling and Software, July. http://www.scopus.com/inward/record.url?eid=2-s2.0-84858682542&partnerID=tZOtx3y1

Takagi, T., & Sugeno, M. (1985). Fuzzy identification of systems and its applications to modeling and control. *IEEE Transactions on Systems, Man, and Cybernetics, SMC-15* (1), 116–132. https://doi.org/10.1109/TSMC.1985.6313399

Xiong, L., Shamseldin, A. Y., & O'Connor, K. M. (2001). A non-linear combination of the forecasts of rainfall-runoff models by the first-order Takagi-Sugeno fuzzy system. *Journal of Hydrology*, *245*(1–4), 196–217. https://doi.org/10.1016/S0022-1694(01)00349-3